Desalination and Water Treatment
www.deswater.com

doi: 10.5004/dwt.2019.24593

167 (2019) 156–169
November

Degradation of ciprofloxacin in aqueous solution by activating the peroxymonosulfate using graphene based on $CoFe_2O_4$

Hamidreza Pourzamani[a], Ehsan Jafari[a], MostafaSalehi Rozveh[b], Hamed Mohammadi[c], Mina Rostami[a], Nezamaddin Mengelizadeh[d,*]

[a]*Department of Environmental Health Engineering, School of Health, Environment Research Center, Isfahan University of Medical Sciences, Isfahan, Iran, emails: Pourzamani@hlth.mui.ac.ir (H. Pourzamani), Ehsanjafari12@yahoo.com (E. Jafari), Rostami69mina@yahoo.com (M. Rostami)*

[b]*Department of nanotechnology engineering, Faculty of advanced science and technology, Isfahan University, Isfahan, Iran, email: Iranianmachine@gmail.com*

[c]*Department of Environmental Health Engineering, Torbat Jam Faculty of Medical Sciences, Torbat Jam, Iran, email: mohammadih2@trjums.ac.ir*

[d]*Department of Environmental Health Engineering, Evas Faculty of Health, Larestan University of Medical Sciences, Larestan, Iran, Tel. +98-939-231-2472; email: Nezam_m2008@yahoo.com*

Received 24 October 2018; Accepted 20 June 2019

ABSTRACT

In this study, the graphene-cobalt ferrites (G-$CoFe_2O_4$) nanocatalyst was synthesized and used to activate peroxymonosulfate (PMS) for the degradation of ciprofloxacin (CIP). The scanning electron microscopy and powder X-ray diffraction analysis results showed the successful loading of $CoFe_2O_4$ on the graphene surface. The effect of operational parameters such as initial pH, G-$CoFe_2O_4$ dosage, PMS dosage and initial concentration of ciprofloxacin on CIP degradation efficiency and the kinetic constant rate was evaluated. The results showed that highest removal efficiency of CIP was achieved at pH 7, 200 mg/L G-$CoFe_2O_4$, 2 mM PMS, 25 mg/L CIP and 30 min reaction time. The results also showed that the PMS/G-$CoFe_2O_4$ system works in a wide range of pH (4–7) with a minimum reduction in degradation efficiency. The PMS/G-$CoFe_2O_4$ system has a higher efficiency in PMS activation and CIP degradation compared with other catalytic processes. This increase was due to the increase of active sites to adsorb CIP and catalytic degradation of it by radicals. Scavenging experiments using tert butyl-alcohol and ethanol showed that both radicals sulfate ($SO_4^{\bullet-}$) and hydroxyl ($^{\bullet}OH$) are produced in the reaction and the $SO_4^{\bullet-}$ is the main radical for the CIP degradation. The results of continuous experiments showed the high efficiency of the PMS/G-$CoFe_2O_4$ process (91.9%) in CIP degradation. The G-$CoFe_2O_4$ nanocatalyst as the heterogeneous activator of PMS showed the high structural stability, good reusability, high catalytic activity and easy separation by the magnetic field.

Keywords: Ciprofloxacin; Peroxymonosulfate; G-$CoFe_2O_4$; Degradation

1. Introduction

In recent years, the use of active pharmaceutical compounds has led to an increase in their discharge into the water body and also to remain in aquatic environments [1,2]. Ciprofloxacin (CIP) is one of the most important classes of fluoroquinolone antibiotics based on annual global sales and therapeutic versatility [3]. These drugs are widely used in the control of human and animal diseases, such as urinary, respiratory and fungal infections, and are commonly

* Corresponding author.

found in the natural water body, pharmaceutical and hospital wastewaters in concentrations of ng/L to mg/L [3–6]. Due to having the carbostyril nucleus with high chemical stability, these antibiotics are not completely metabolized in the body and more than 70% of them are released without metabolizing [6,7]. In addition, these compounds are typically stable in the biological process, which results in the continuous discharge of CIP into the environment through the wastewater treatment plant [5]. The long-term exposure to environmental concentrations of CIP causes serious health problems for humans and the ecosystem by inducing proliferation of bacterial drug resistance [8]. Therefore, the effective elimination of this pollutant and reduction of its environmental effects are necessary.

Recently, various treatment processes such as adsorption [9] and membrane process [10] have been used to remove CIP from aqueous solutions. However, these methods have disadvantages such as low efficiency, membrane clogging, secondary pollutant generation and transmission of contamination from one phase to another [4]. In contrast, the advanced oxidation processes (AOPs) have newly attracted the considerable attention due to easy use, high efficiency, low cost and generation of reactive species with high oxidative potential, such as $SO_4^{\bullet-}$ and $^{\bullet}OH$ [11,12]. Among the AOPs, activated peroxymonosulfate (PMS) oxidation has been considered due to its high efficiency, high chemical resistance than to H_2O_2, and rapid activation than to persulfate anions in the organic pollutants treatment process [12–14]. In this process, $SO_4^{\bullet-}$ along with $^{\bullet}OH$ is produced by catalytic degradation of PMS in a pathway with the help of transition metal, UV radiation and ultrasonic [15]. In recent years, the use of ultrasonic, heat and UV for the activation of PMS has not been economical, while transition metals have a high performance for PMS activation [14]. Various transition metals such as Co, Fe, Mn, Cu and Ag have been widely used to activate the PMS in the homogeneous forms [12,14]. Among the catalysts, cobalt metal has attracted a lot of attention due to the rapid activation of PMS and the acceleration of contaminant degradation in short time (Eqs. (1)–(3)) [16]. However, the use of the PMS/Co system has limitations such as cobalt toxicity, recycling and its hard separation [14,17–19]. To dominate these problems, researchers have proposed the use of magnetite cobalt ferrite hybrid ($CoFe_2O_4$) due to its ferromagnetic characteristics, high chemical and thermal stability, stable crystalline structure and excellent mechanical hardness [20,21]. The satisfactory catalytic activity of the $CoFe_2O_4$ nanocatalyst in the activation of PMS and the degradation of various pollutants was confirmed by other studies [22]. For example, Tan et al. [23] investigated the degradation of the paracetamol using the $CoFe_2O_4$ as the PMS heterogeneous catalyst. The authors found that $CoFe_2O_4$ has high activity in activating the PMS and producing reactive species such as $SO_4^{\bullet-}$ and $^{\bullet}OH$. In addition, Xu et al. [24] showed that the excellent catalytic performance of $CoFe_2O_4$ in the activation of PMS and complete degradation of bisphenol A in 60 min. Although this nanocatalyst showed good activity in the decomposition and activation of PMS, its considerable accumulation due to the high ratio of surface area to volume is a problem for technological applications [18,25]. Recently, the support for the $CoFe_2O_4$ catalyst was proposed as a method to provide better dispersion in the water and a higher rate of particle distribution [26,27]. Various supports such as mesoporous carbon [28], clay [29] and zeolite [30] were used to prepare the $CoFe_2O_4$ catalyst. In contrast, the graphene showed high performance in support of various catalysts, especially $CoFe_2O_4$, due to its remarkable properties with many functional groups [21,31]. Graphene is a hydrophobic and non-polar material with a two-dimensional crystal structure that is widely used to remove the various pollutants such as antibiotics [20,21]. This substance due to the characteristics including high surface area, extraordinary electronic transport, high physical and chemical stability and the excellent adsorption has the ability to increase the pollutant removal and its degradation through the adsorption-catalysis process [17,31]. To prove, it has recently reported that the graphene composites with TiO_2, Co_3O_4, MnO_4 and ZnO nanoparticles have high activity in the electrochemical catalyst, photocatalytic degradation and capacitors with minimal leaching of nanoparticles [17].

$$Co^{2+} + HSO_5^- \rightarrow CO^{3+} + SO_4^{-\bullet} + OH^- \quad (1)$$

$$SO_4^{-\bullet} + H_2O \rightarrow SO_4^{2-} + {}^{\bullet}OH + H^+ \quad (2)$$

$$SO_4^{-\bullet} \text{ or } {}^{\bullet}OH + \text{Pollutant} \rightarrow \text{intermediate} + CO_2 + H_2O \quad (3)$$

The purpose of the present study was to synthesize the graphene based on the magnetic nanocomposite (G-$CoFe_2O_4$) and to investigate its effectiveness in the activation of PMS and degradation of CIP. The physicochemical properties of the synthesized catalyst were characterized by scanning electron microscopy (SEM), transmission electron microscopy (TEM), electron dispersive X-ray spectroscopy (EDX), powder X-ray diffraction (XRD), and pH of the zero point of charge (pHzpc) analysis. The effect of different parameters such as initial pH, dosage of G-$CoFe_2O_4$ catalyst, dosage of PMS, initial concentration of CIP and reaction time were investigated. Trapping experiments were carried out to probe the active reactive species in the PMS/G-$CoFe_2O_4$ system. The stability and reusability of G-$CoFe_2O_4$ nanoparticles were investigated through catalytic reaction cycles and XRD and EDX analysis. The CIP degradation pathway was proposed based on the by-product identified by liquid chromatography-mass spectrometry. Finally, column tests were evaluated for the feasibility of the PMS/G-$CoFe_2O_4$ process in the treatment of CIP-containing solution. The contribution of this study was the evaluation of the use of oxidation columns in the CIP degradation that was not found in previous studies.

2. Materials and methods

2.1. Materials

Ciprofloxacin (CIP, $C_{17}H_{18}FNO_3O_3$, 98%) was purchased from Sigma-Aldrich Co., USA. Ferric nitrate nonahydrate ($Fe(NO_3)3{\cdot}9H_2O$), cobalt nitrate hexahydrate ($Co(NO_3)2{\cdot}6H_2O$), sodium hydroxide (NaOH), methanol (CH_3OH) and tert-butyl alcohol (TBA) were obtained from Merck Co., Germany. Oxone (PMS, $2KHSO_5{\cdot}KHSO_4{\cdot}K_2SO_4$) was purchased from Sigma-Aldrich Company and was used as

an oxidant without purification. HPLC-grad acetonitrile was purchased from Merck Co., Germany. All the materials used in this study were of analytical grade. Graphene oxide (carbon purity, GO = 99%, surface area = 100–300 m^2/g, thickness = 3.4–7 nm) was purchased from US Research Nanomaterials (Lauisiana, USA).

2.2. Synthesis of G-$CoFe_2O_4$

The G-$CoFe_2O_4$ catalyst was synthesized with $Co(NO_3)_2 \cdot 6H_2O$ and $Fe(NO_3)_3 \cdot 9H_2O$ precursors and Xu et al. [20] method. 0.3 g of graphene oxide (GO) in 100 mL distilled water was dispersed with ultrasonic to prepare a homogeneous suspension. Then 2.02 g of $Fe(NO_3)_3 \cdot 9H_2O$ and 0.73 g of $Co(NO_3)_2 \cdot 6H_2O$ dissolved in 20 mL water were added to the GO solution at room temperature with continuous mixing. After adding NaOH (1 M) to the mixture in the water bath at the temperature of 80°C, its pH value was adjusted to above 12. Then, 8 mL of hydrazine hydrate was added to the solution during the constant stirring to reduce GO to graphene and, as a result, a black solution was obtained. Afterward, the solution containing nanocatalyst was stirred at room temperature for its cooling. The solid was separated by centrifugation and was completely washed with water and ethanol to remove the impurities. Finally, the nanocatalyst was dried in an oven vacuum at 60°C for 24 h.

The crystalline structure of G-$CoFe_2O_4$ nanocatalyst was determined using powder XRD using Cu-Ka radiation. Sample morphology was characterized by SEM and TEM. The energy dispersive X-ray spectroscopy was used for the analysis of the composition of the nanocatalyst. Zeta potential of catalyst was measured in various pH values (2–12) using a Zetasizer (Nano-ZS, Malvern Instruments Ltd., Malvern, UK).

2.3. Experimental methods

To evaluate the PMS/G-$CoFe_2O_4$ system in CIP degradation, batch experiments were carried out in 250 mL conical flasks under mechanical stirring at room temperature (25°C ± 1°C). In this study, the effect of the experimental parameters was evaluated by varying one factor and keeping constant of other factors. In each run, various amounts of G-$CoFe_2O_4$ nanocatalysts (50–500 mg/L) were added to 100 mL of CIP solution at an initial concentration of 10–100 mg/L. Also, a different dosage of PMS (0.5–4 mM) was added to a solution containing a constant pH. At different times, 1 mL of solution was withdrawn using 5 mL syringe and the nanocatalyst was separated by a magnetic field. Then, 0.5 mL of methanol was added to the extracted solution to quench the reaction, and the remaining CIP concentration was analyzed by the HPLC with a UV detector at 275 nm. 40% acetonitrile and 60% distilled water were used as mobile phase at a flow rate of 0.75 mL/min. Identification of intermediates was performed by liquid chromatography coupled with a mass spectrometer (LC–MS) [32].

Column tests were performed to verify the CIP removal efficiency by activated PMS. A plexiglass column with a diameter of 5 cm and a length of 20 cm was filled with stainless steel wool (Fig. 1). Finally, the column was operated based on the optimum condition obtained in the batch conditions with the contact time of 5, 10, 20 and 30 min. To survey the stability and reusability, the regenerated nanocatalyst was washed several times with distilled water and then was dried at 70°C and was finally added to the solution with the previous optimum conditions. To determine the kinetic constant rate of CIP degradation by the PMS/G-$CoFe_2O_4$ system, the first-order kinetic model (Eq. (4)) was used. The ciprofloxacin degradation efficiency was calculated according to Eq. (5). Moreover, the relative contributions of reactive species for CIP degradation were determined as follows:

$$\mathrm{Ln}\left(\frac{C_0}{C_e}\right) = Kt \tag{4}$$

$$\%\ \mathrm{Degradation} = \left(\frac{C_0 - C_e}{C_0}\right) \times 100 \tag{5}$$

$$\text{Contribution of } SO_4^{-\bullet} \text{ or } {}^{\bullet}OH = \frac{\text{degradation efficiency with } SO_4^{-\bullet} \text{ or } {}^{\bullet}OH \text{ scavenger}}{\text{degradation efficiency without scavenger}} \times 100 \tag{6}$$

where K is the first order constant rate of CIP degradation, t is the reaction time, C_0 and C_e are the initial and final concentration of CIP, respectively.

3. Results and discussion

3.1. Characteristics of G-$CoFe_2O_4$

To study the morphology and catalyst structure, SEM and TEM images were taken for synthesized G-$CoFe_2O_4$. The graphene morphology is clearly visible in Figs. 2a and 3a. The figures show a large number of fine particles formed on the graphene layer structure. The EDX analysis (Fig. 4)

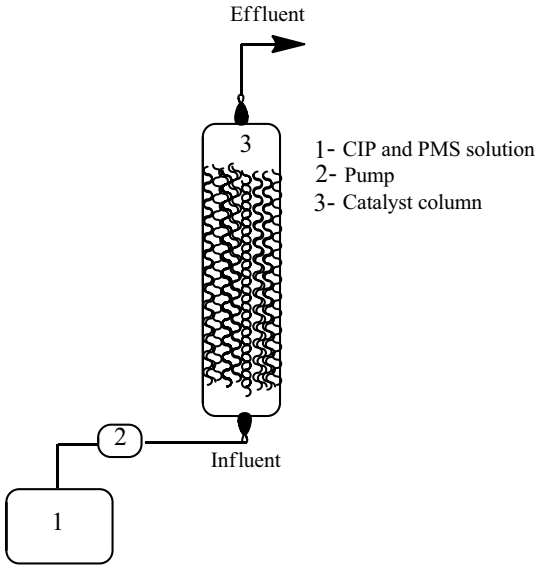

Fig. 1. Up-flow column used for continuous experiments.

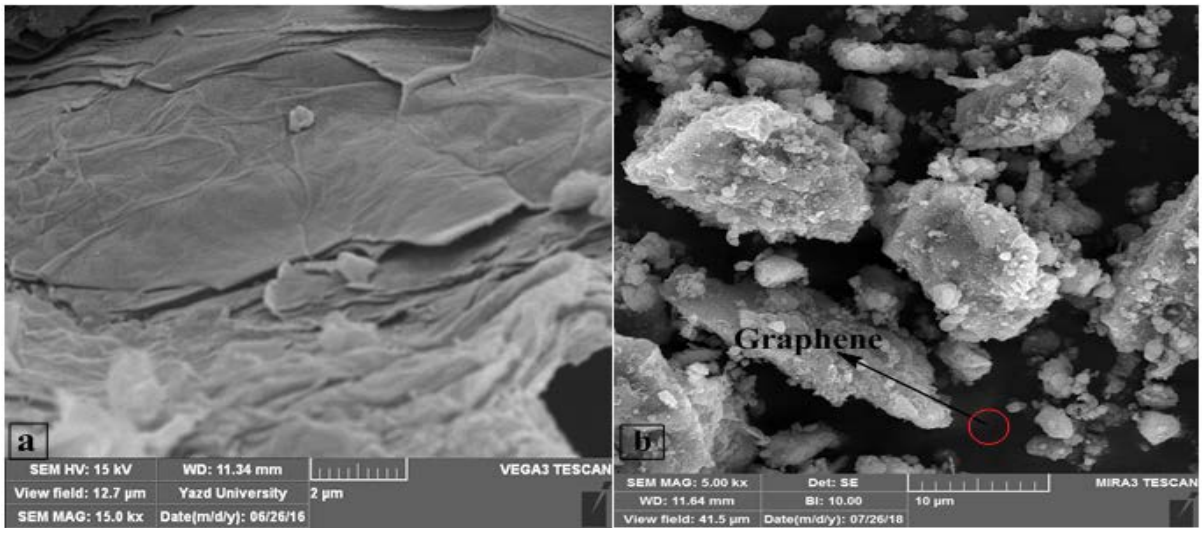

Fig. 2. SEM images of (a) graphene and (b) G-$CoFe_2O_4$.

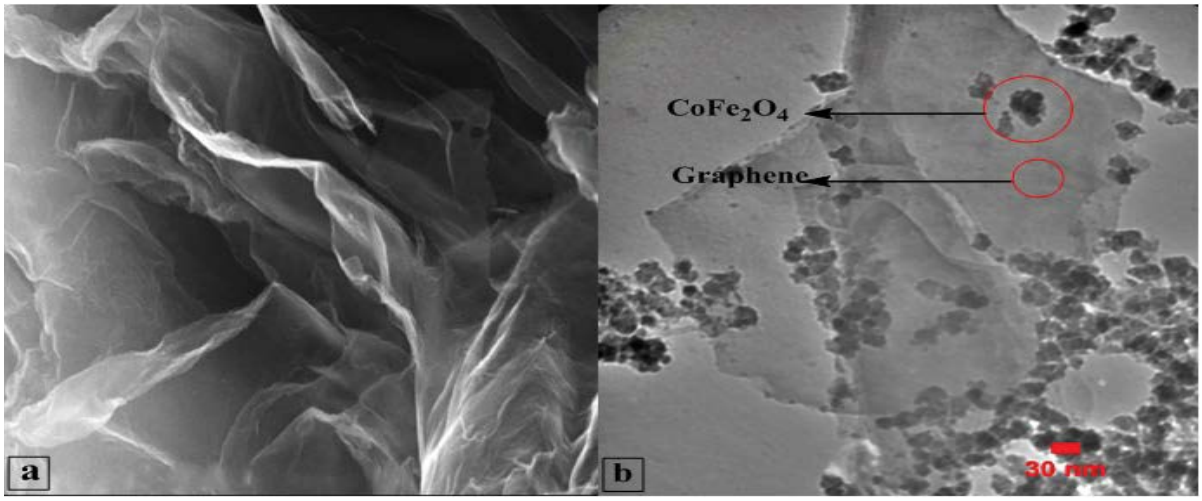

Fig. 3. TEM images of (a) graphene and (b) G-$CoFe_2O_4$.

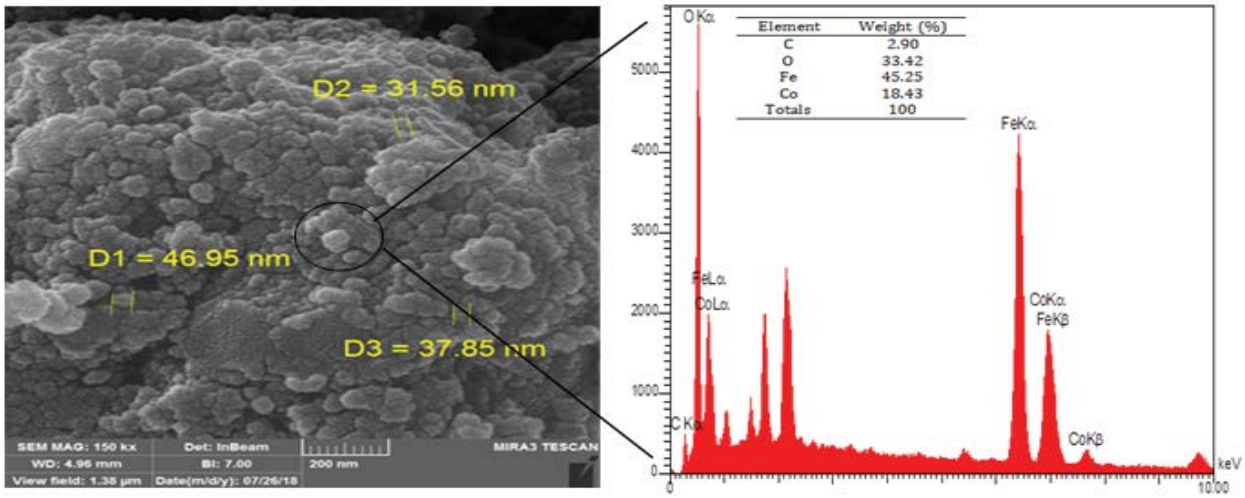

Fig. 4. EDX spectra of synthesized G-$CoFe_2O_4$.

based on the identification of cobalt, iron and oxygen proved that the G-$CoFe_2O_4$ catalyst with the size of 30–45 nm is comprised.

The phase and structure of the synthesized catalyst were determined by XRD analysis. As shown in Figs. 5a and b, the strong peak at 2θ = 10.28° is related to graphene, while the peaks at 2θ = 30.13°, 35.53°, 43.38°, 53.5°, 57.05° and 62.66° are related to the cobalt ferrite structure. Moreover, it can be seen that diffraction peaks of graphene could not be identified in the XRD pattern of G-$CoFe_2O_4$, showing the destruction of the structure of graphene due to the crystal growth of $CoFe_2O_4$ between its layers. These results indicate that the G-$CoFe_2O_4$ catalyst has been successfully prepared. Similar results were observed for the synthesis of $CoFe_2O_4$ by Gan et al. [33]. Fig. 6 shows the Raman spectra of graphene, $CoFe_2O_4$ and G-$CoFe_2O_4$. According to this figure, the Raman spectra of G-$CoFe_2O_4$ were containing graphene peak and $CoFe_2O_4$, which represents a good synthesis of nanocatalyst by co-precipitation method.

3.2. Effect of solution pH

The initial pH is one of the most important parameters on the CIP dissociation, the surface properties of the catalyst and the formation of active species [34–36]. The effect of initial solution pH on the PMS/G-$CoFe_2O_4$ process was investigated in the pH range of 2–10 and the results are shown in Fig. 7. According to this figure, the optimum performance occurs within the pH range of 4–7. The removal efficiency in this range was between 81.27% and 95.11%, and the kinetic constant rate varies from 0.0178 to 0.0417 min^{-1} (Table 1). However, the CIP removal was decreased to 60.1% and the kinetic constant rate to 0.0074 min^{-1} by increasing the solution pH to 10. In addition, the removal of CIP and the kinetic constant rate at a highly acidic pH (pH = 2) is significantly changed compared with optimum pH. Increasing the CIP removal efficiency and the high kinetic rate at pH between 4 and 7 can be related to facilitating the adsorption and degradation process by electrostatic adsorption

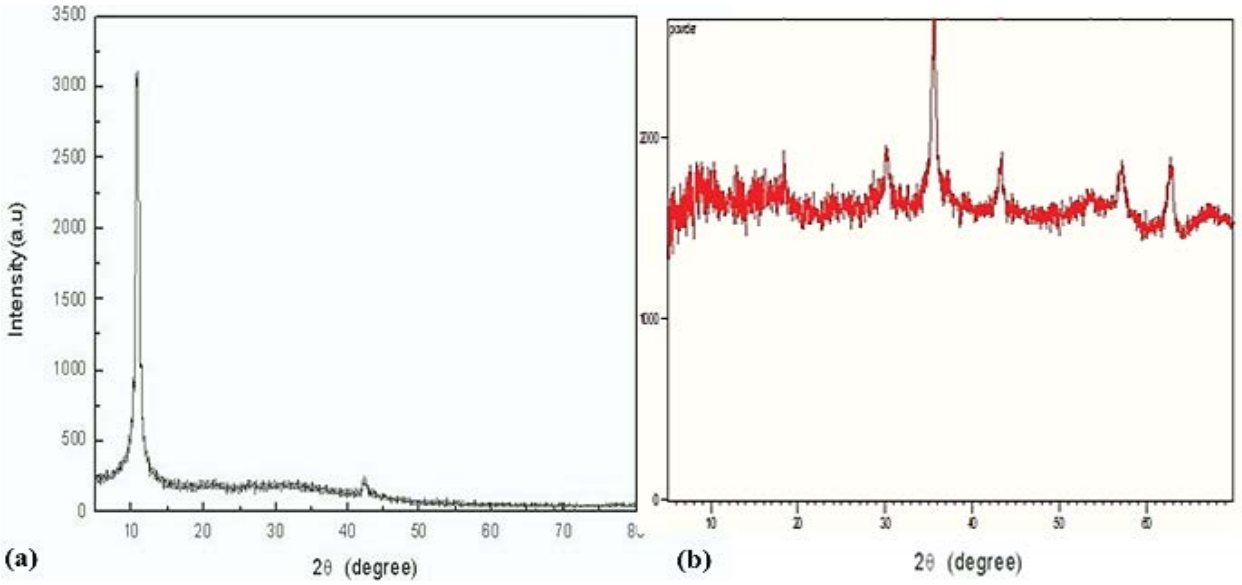

Fig. 5. XRD patterns of (a) graphene, and (b) G-$CoFe_2O_4$.

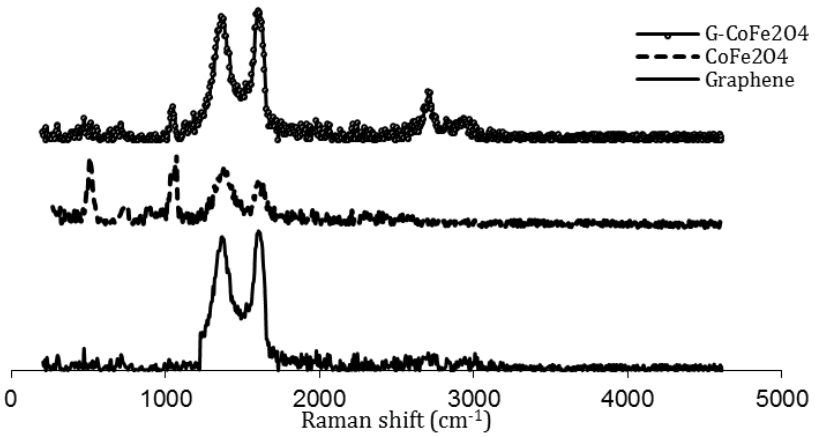

Fig. 6. Raman spectra of graphene, $CoFe_2O_4$ and G-$CoFe_2O_4$.

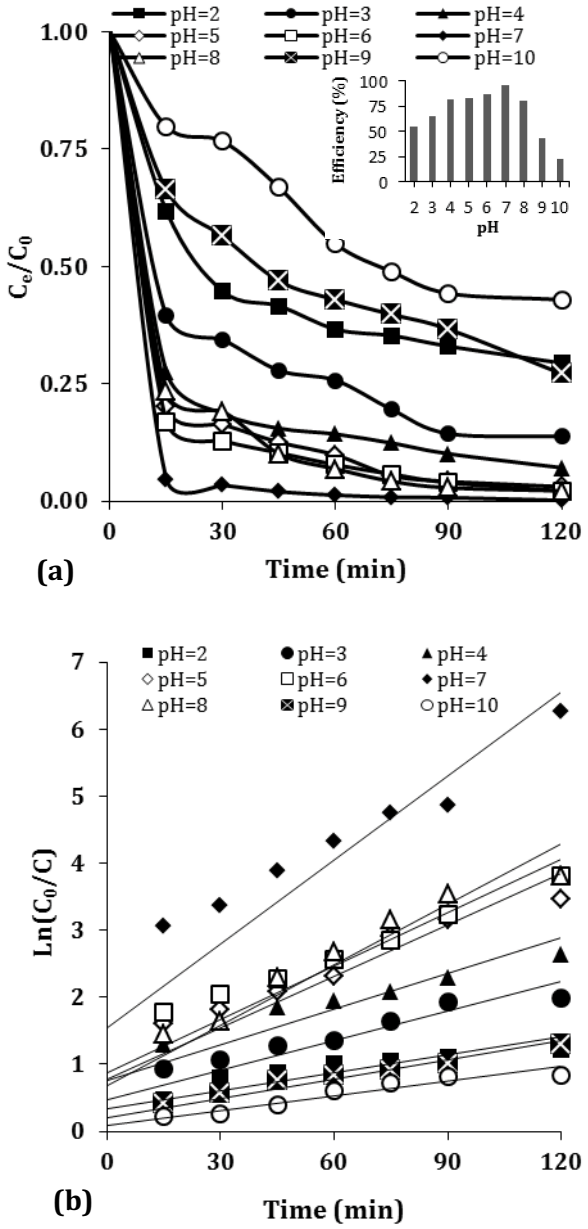

Fig. 7. (a) CIP degradation at different pH in PMS/G-$CoFe_2O_4$ system. (Inset indicates CIP degradation in min) and (b) kinetic curves (catalyst dosage = 250 mg/L, PMS dosage = 2 mM, CIP concentration = 25 mg/L).

Table 1
Kinetic parameters for different operating conditions

Parameters	k/min^{-1}	R^2
pH	Other conditions: D_{cat} = 250 mg/L, D_{PMS} = 2 mM, C_0 = 25 mg/L	
2	0.0089	0.797
3	0.0148	0.855
4	0.0178	0.785
5	0.0255	0.870
6	0.0265	0.860
7	0.0417	0.826
8	0.0301	0.912
9	0.0096	0.930
10	0.0074	0.937
Catalyst dosage (mg/L)	Other conditions: pH = 7, D_{PMS} = 2 mM, C_0 = 25 mg/L	
50	0.0097	0.982
75	0.0153	0.825
100	0.0165	0.835
150	0.0215	0.822
200	0.0325	0.820
500	0.0509	0.862
PMS dosage (mg/L)	Other conditions: pH = 7, D_{cat} = 200 mg/L, C_0 = 25 mg/L	
0.5	0.0062	0.928
0.75	0.0162	0.947
1	0.0226	0.987
1.25	0.0239	0.969
1.5	0.0247	0.947
2	0.0562	0.973
4	0.0662	0.945
CIP concentration (mg/L)	Other conditions: pH = 7, D_{cat} = 200 mg/L, D_{PMS} = 2 mM	
10	0.0632	0.974
25	0.0554	0.977
50	0.0240	0.984
100	0.0121	0.875

Note: D_{cat} = G-$CoFe_2O_4$ dosage; C_0 = initial CIP concentration, D_{PMS} = PMS dosage.

between the G-$CoFe_2O_4$ surface and the CIP molecules [37]. The point of zero charge (PZC) of the synthesized catalyst and the pKa_2 ciprofloxacin [38] were 2.7 and 8.24, respectively. Therefore, when pH > PZC, the better interaction between G-$CoFe_2O_4$ and CIP occurs and the oxidation of the pollutant increases due to the access to the catalyst surface. These results agree with most of the previous studies, such as 2,4-dichlorophenol degradation in PMS/Co system [39], Rhodamine B oxidation in PMS/$CoFe_2O_4$/TNTs [26] and diclofenac degradation in PMS/$CoFe_2O_4$ system [22].

Decreasing the degradation efficiency and the kinetic constant rate at alkaline pH can be explained by changing the cobalt species from Co(II) to Co(III) or the self-dissociation of PMS through the non-radical path [40]. Do et al. [41] reported that the Co(III) has a smaller ability in the activation of the PMS to produce the $SO_4^{\bullet}$ compared with Co(II). In addition, the CIP degradation efficiency decrease in the alkaline pH is due to the presence of HCO_3^- and CO_3^{2-} as the scavenger of the reactive species [42]. Xu et al. [20] evaluated the PMS/G-$CoFe_2O_4$ system for the degradation of dimethyl phthalate and reported that the highest degradation of the pollutant occurred in the range of 4–8.35 and the removal of dimethyl phthalate was reduced at the alkaline pH due to the

conversion of $SO_4^{\bullet}$ to $_{\bullet}O^-$ (Eqs. (7) and (8)). Huang et al. [43], in addition to prove the above results, reported that the removal of methylene blue in high pH is due to the production of $^{\bullet}OH$ by oxidizing OH^- or H_2O (Eq. (7)) by $SO_4^{\bullet}$ produced by PMS/Co.

Decreasing the degradation efficiency and the kinetic constant rate at a highly acidic pH is related to the scavenging effect of hydrogen ion (H^+) for $SO_4^{\bullet-}$ and $^{\bullet}OH$ (Eqs. (9) and (10)) and the formation of H-bond between H^+ and O–O group of PMS that prevents the reaction between the PMS and the catalyst surface [19,42]. Su et al. [44] reported the PMS heterogeneous activity by $Co_xFe_{3-x}O_4$ for Rhodamine B degradation. The authors found that the highest removal efficiency occurred at pH between 5 and 6 and its removal efficiency reduced at pH < 3 due to the lack of activation of PMS by the nanocatalyst.

$$SO_4^{-\bullet} + OH^- \rightarrow SO_4^{2-} + {}^{\bullet}OH \quad (7)$$

$$OH^{\bullet} + H_2O \rightarrow {}_{\bullet}O^- + H_3O^+ \quad (8)$$

$$^{\bullet}OH + H^+ + e^- \rightarrow H_2O \quad (9)$$

$$SO_4^{-\bullet} + H^+ + e^- \rightarrow HSO_4^{\bullet-} \quad (10)$$

3.3. Effect of G-$CoFe_2O_4$ catalyst dosage

The catalyst dosage is one of the controller parameters for the production of reactive species and the efficiency of the PMS-based oxidation process. The effect of the initial dosage of G-$CoFe_2O_4$ catalyst on the CIP degradation efficiency and first-order kinetic constant rate under the conditions including pH of 7, PMS dosage of 2 mM and CIP concentration of 25 mg/L are shown in Fig. 8. As shown, G-$CoFe_2O_4$ has a significant effect on CIP degradation. With increasing the catalyst dosage from 50 to 500 mg/L, the efficiency of CIP degradation was increased dramatically. When the catalyst dosage was 50 mg/L, 67.87% of CIP was eliminated during 120 min, while the degradation efficiency reached 97.65% using catalyst dosage of 500 mg/L over a period of 30 min. Kinetically, *K* was increased from 0.0097 to 0.0509 min^{-1} when G-$CoFe_2O_4$ dosage increased from 50 to 500 mg/L (Table 1). This increase may be related to an increase in the number of active sites for adsorption of CIP and production of more functional radicals [20,44,45]. Similar results were observed in phenol degradation using a Fe_3O_4/carbon sphere/cobalt composite as a PMS heterogeneous catalyst [18]. The results of Fig. 8 show that the CIP removal efficiency at dosage of 200 and 500 mg/L during the 30 min is not significant. Considering the economic cost and practical application, 200 mg/L of G-$CoFe_2O_4$ catalyst was selected for further CIP degradation experiments.

3.4. Effect of PMS dosage

The effect of the PMS dosage on the CIP degradation efficiency was investigated and the results are shown in Fig. 9. As it can be observed, the CIP degradation efficiency was increased from 30.452% to 96.57% by increasing the PMS dosage from 0.5 to 4 mM. At the same time, the kinetic constant rate was increased from 0.0062 to 0.0662 min^{-1} (Table 1). These results can be explained by this fact that increasing the dosage of PMS leads to increase its chances to react with G-$CoFe_2O_4$, which improves the PMS activation rate for producing the reactive species and further degradation of CIP [46]. Similar results were observed for the degradation of organic pollutants by Zhou et al. [47], Su et al. [44] and Lai et al. [48].

The results in Fig. 9a show that by increasing the PMS dosage from 2 to 4 mM, the increase in CIP removal efficiency

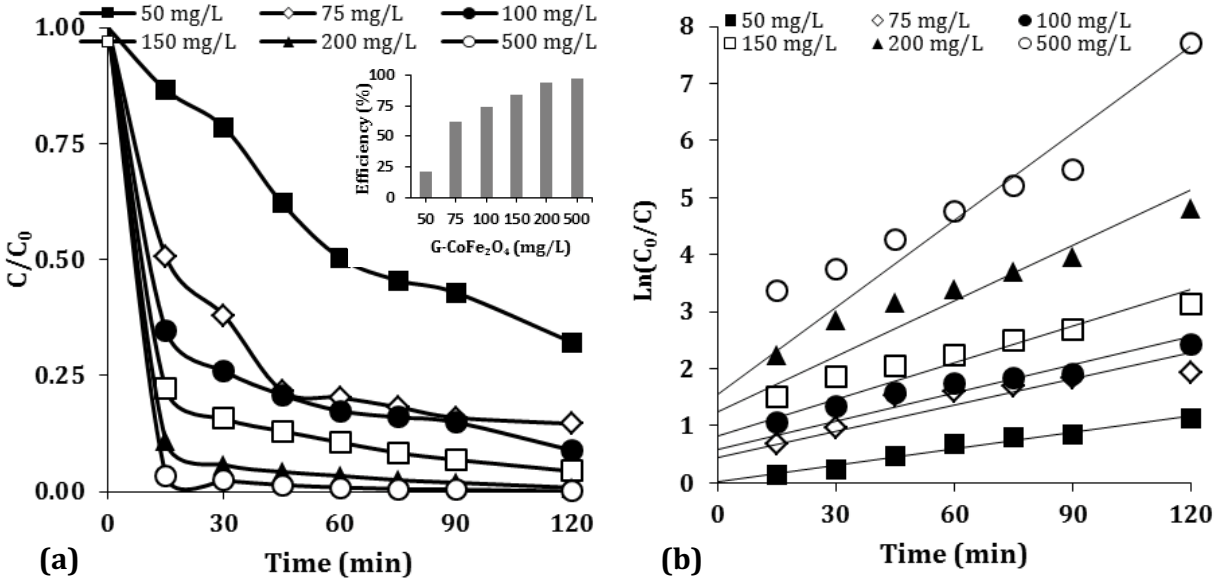

Fig. 8. (a) CIP degradation at different dosages of catalysts in PMS/G-$CoFe_2O_4$ system (inset indicates CIP degradation in 30 min) and (b) kinetic curves (initial pH = 7, PMS dosage = 2 mM, CIP concentration = 25 mg/L).

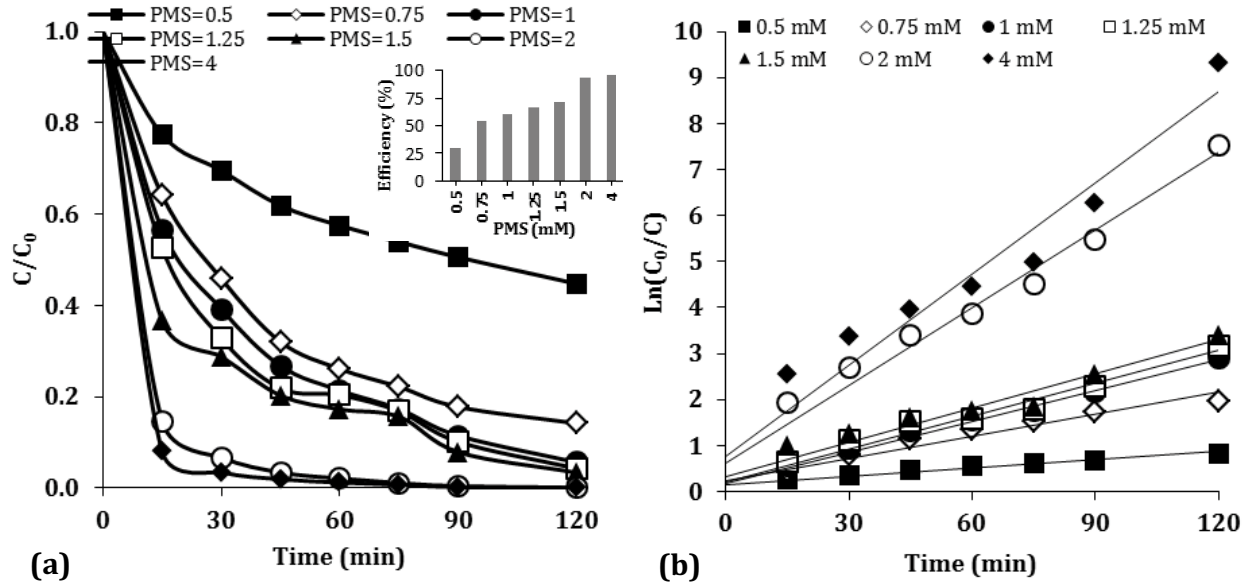

Fig. 9. (a) CIP degradation at different dosages of PMS in PMS/G-$CoFe_2O_4$ system (inset indicates CIP degradation in 30 min) and (b) kinetic curves (initial pH = 7, catalyst dosage = 200 mg/L, CIP concentration = 25 mg/L).

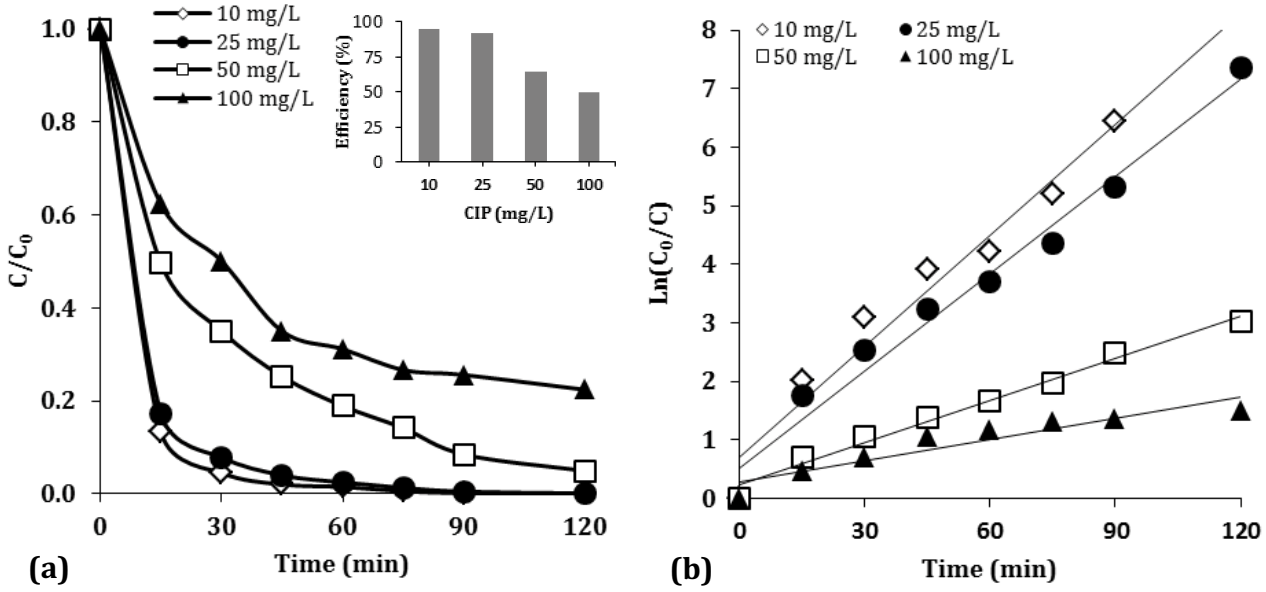

Fig. 10. (a) CIP degradation at different concentrations of CIP in PMS/G-$CoFe_2O_4$ system (inset indicates CIP degradation in 30 min) and (b) kinetic curves (initial pH = 7, catalyst dosage = 200 mg/L, PMS dosage = 2 mM).

is negligible. Therefore, considering the economic cost, PMS dosage of 2 mM was selected as a suitable oxidant concentration for subsequent experiments.

3.5. Effect of CIP concentration

The effect of the initial concentration of CIP (10–100 mg/L) on the CIP degradation efficiency is shown in Fig. 10. As can be seen, the CIP degradation efficiency decreases with increasing the initial concentration of CIP. In reaction time of 60 min, the removal efficiency can reach 98.59% for an initial concentration of 10 mg/L of CIP, while at the same time, the CIP removal efficiency at the concentration of 25, 50 and 100 mg/L is decreased to 97.55%, 81.1% and 68.86%, respectively. The kinetic constant rate, such as the CIP degradation efficiency, was decreased from 0.0632 to 0.0121 min^{-1} by increasing the CIP concentration (Table 1). This decrease can be due to the limitation of active species in the oxidation system for high concentrations and the competition between intermediate products and CIP molecules for $SO_4^{\bullet-}$ and $^{\bullet}OH$ produced. Similar results were reported for the degradation of dimethyl phthalate by the PMS/G-$CoFe_2O_4$ system

[46] and acetaminophen degradation by the PMS/Fe_3O_4 system [49].

3.6. Catalytic activity of G-$CoFe_2O_4$

Fig. 11 shows the CIP degradation curves under different conditions. No CIP degradation was observed in the presence of 2 mM alone, which it is suggested that the PMS does not have the capability for the oxidation of CIP in homogeneous solutions. By adding $CoFe_2O_4$ alone to the solution, approximately 10% CIP was removed due to its adsorption on the nanocatalyst surface. At the same time, the adsorption on the G-$CoFe_2O_4$ was 2.24 times higher than that of $CoFe_2O_4$. This is probably due to the presence of graphene. Previous studies reported that graphene is a support substance in heterogeneous catalyst systems, which can improve the efficiency of oxidation and adsorption processes by increasing the contact surface [50]. Adding graphene to a solution containing CIP and PMS increases the CIP degradation efficiency to 47.18% at 120 min. Xu et al. [20] reported that this

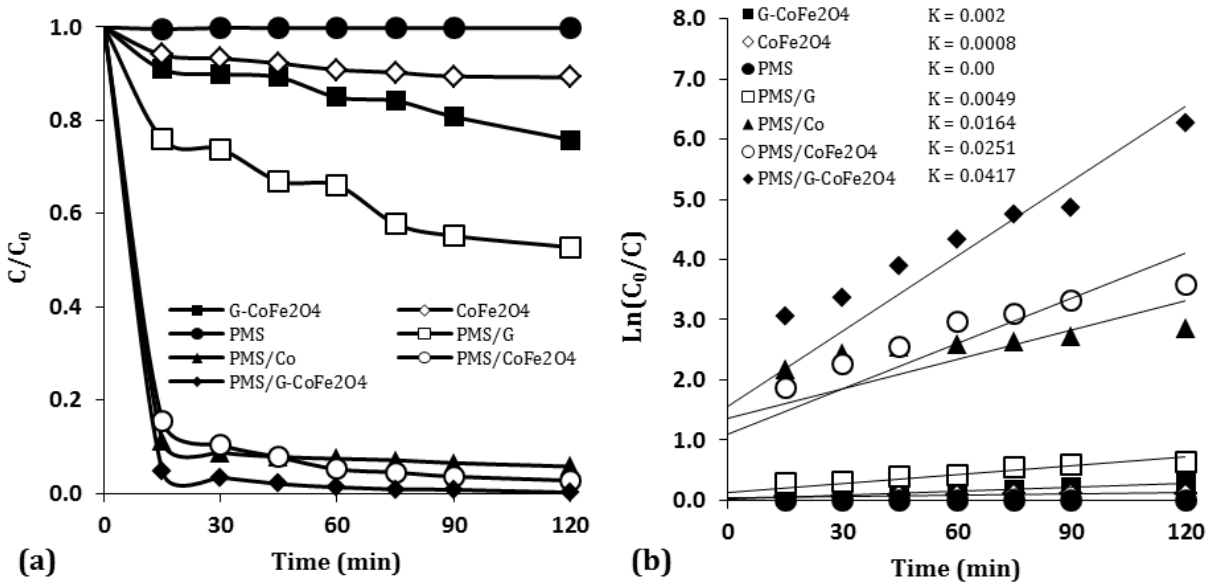

Fig. 11. (a) Degradation curves of CIP under different conditions and (b) kinetic curves (initial pH = 7, catalyst dosage = 200 mg/L, PMS dosage = 2 mM, CIP concentration = 25 mg/L).

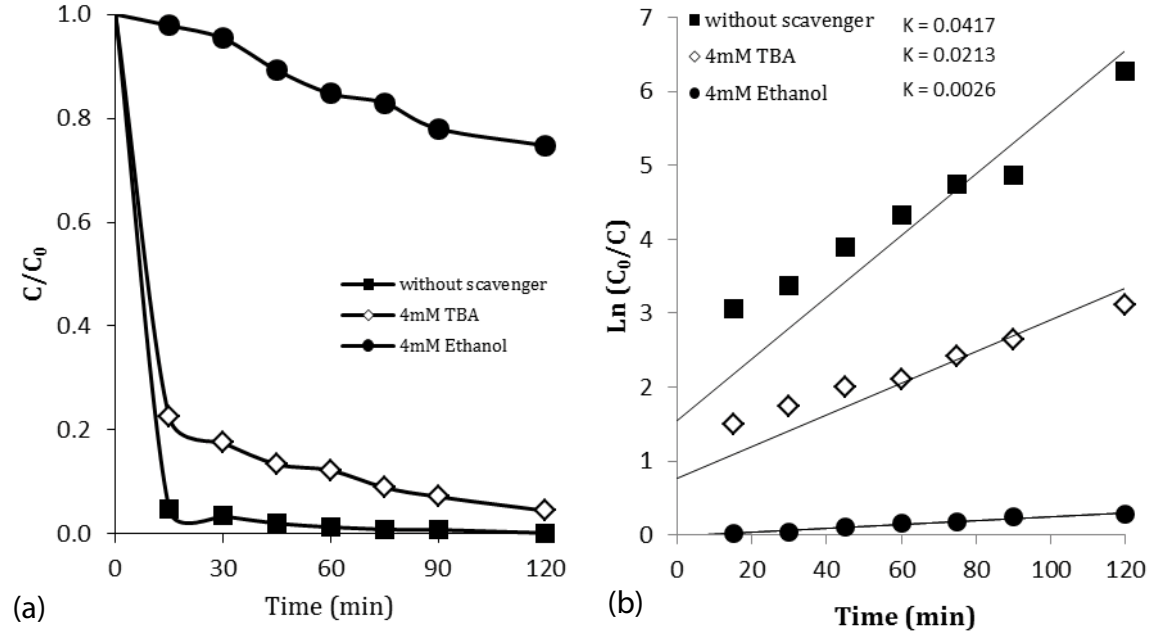

Fig. 12. (a) CIP degradation changes in the presence of different scavengers and (b) kinetic curves (initial pH = 7, catalyst dosage = 200 mg/L, PMS dosage = 2 mM, CIP concentration = 25 mg/L).

increase in efficiency is due to the electrostatic adsorption between the π-π conjugation region of the graphene layers and the pollutant molecules. To prove this fact, they added the methanol to the solution and found that 87% of the pollutants are eluted from the graphene surface. The results of Fig. 11 also show that the CIP removal efficiency in the PMS/Co homogeneous system at the initial time (15–45 min) was much higher than the $CoFe_2O_4$ system, but, in the long-term, the removal rate was fixed and this homogenous system was not able to provide the complete degradation compared with heterogeneous catalyst. In the PMS/Co system, the homogeneous cobalt can quickly react with PMS and can lead to faster production of reactive species. This rapid production of radicals leads to their loss by reaction with non-target molecules [24]. In contrast, the catalytic performance of $CoFe_2O_4$ system over a long period of time, by controlling the production of radicals, leads to greater degradation of the CIP than the PMS/Co. Compared with all of the above processes, it is seen that the CIP degradation rate is much faster and more efficient using the PMS/G-$CoFe_2O_4$ system. These results emphasize the critical role of interaction between graphene and $CoFe_2O_4$ on the G-$CoFe_2O_4$ nanocatalysts. Such an increase in catalytic activity can be attributed to increasing the active site for catalytic degradation of CIP

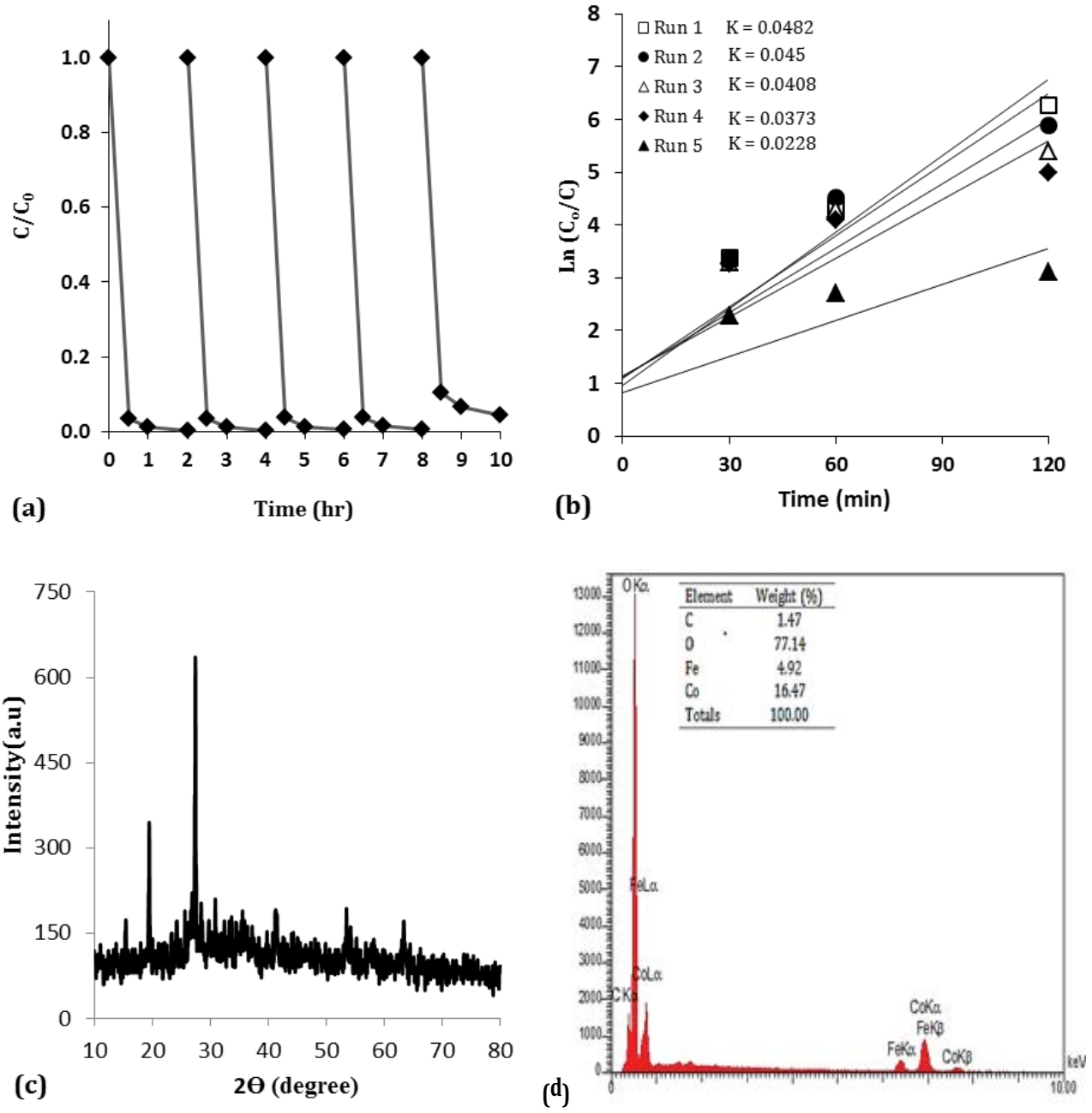

Fig. 13. (a) Degradation of CIP in consecutive run cycles using the recycled G-$CoFe_2O_4$, (b) Kinetic curves, (c) XRD patterns, and (d) EDX spectra.

and to preventing the accumulation of $CoFe_2O_4$ nanoparticles by graphene [46]. Similar results were observed by Shi et al. [51], Zhou et al. [47] and Yao et al. [46].

3.7. Quenching study to identify the reactive species

Organic compounds are generally degraded through the reactive species produced during the activation of oxidants such as PMS, persulfate, H_2O_2, etc. Hence, it is important to find active reactive species in oxidation to provide the degradation mechanism. In the homogeneous or heterogeneous activation process, PMS, $SO_4^{\bullet-}$, $^{\bullet}OH$ and peroxymonosulfate radical ($SO_5^{\bullet-}$) are produced. According to Deng et al. [22], the $SO_5^{\bullet-}$ radical, with a lower redox potential (1.1 V), does not have the ability to degrade the CIP. Therefore, in order to study the role of $SO_4^{\bullet-}$ and $^{\bullet}OH$ in the degradation of CIP, the TBA and ethanol were added to the PMS/G-$CoFe_2O_4$ system, and the removal efficiency changes are represented in Fig. 12. It has reported that ethanol has high reactivity with $SO_4^{\bullet-}$ (1.6×10^9–$7.7 \times 10^9\ M^{-1}S^{-1}$) and $^{\bullet}OH$ (1.2×10^9–$2.8 \times 10^9\ M^{-1}S^{-1}$), and TBA has a good reactivity with $^{\bullet}OH$ (3.8×10^8–$7.6 \times 10^8\ M^{-1}S^{-1}$) than that $SO_4^{\bullet-}$ (4×10^5–$9.1 \times 10^5\ M^{-1}S^{-1}$) [14]. As shown in Fig. 12, the removal efficiency, at the reaction time of 30 min, was reduced from 96.57% to 82.44% and 4.63% after the addition of TBA and ethanol. At the same time, the kinetic constant rate was decreased from 0.0417 to 0.0213 min^{-1} and 0.0026 min^{-1}. This difference in reduction showed that both $SO_4^{\bullet-}$ and $^{\bullet}OH$ are involved in the degradation of CIP in the PMS/G-$CoFe_2O_4$ system, and the $SO_4^{\bullet-}$ with the participation of more than 80% plays a major role in the oxidation process.

3.8. Stability of G-$CoFe_2O_4$

The stability of the G-$CoFe_2O_4$ nanocatalyst was investigated by conducting five consecutive run cycles (Fig. 13a). After each degradation run, the catalyst was collected by means of a magnetic field, was washed with distilled water and then was dried in an oven at 70°C prior to the next run. It has been observed that the nanocatalyst can be used four times under the same laboratory condition without significant reduction in catalytic activity. After the 4th run, the CIP degradation efficiency was declined from 96.57% to 89.68% within 30 min. The results of the kinetic analysis showed the same trends (Fig. 13b). This can be due to the decrease in the amount of G-$CoFe_2O_4$ in the regeneration process, saturation and destruction of the active catalytic site, as well as leaching the cobalt and Fe from the catalyst surface. These results are in good agreement with the findings of other studies [22,28,44].

In order to confirm the results of stability, XRD analysis was used for the recycled G-$CoFe_2O_4$ after the fourth run. The XRD pattern (Fig. 13c) exhibited a similar structure of G-$CoFe_2O_4$ after the catalytic process. The purity of the G-$CoFe_2O_4$ after the fourth run was confirmed by the EDX, as shown in Fig. 13d. These results show that the G-$CoFe_2O_4$ catalyst have good stability and reusability for the degradation of CIP.

3.9. Continuous experiments

The batch study showed that the G-$CoFe_2O_4$ catalyst has a high potential for PMS activation and CIP degradation from aqueous solutions. However, the batch system is not practical on a real scale for the purification of the aqueous solution containing CIP. Therefore, in the present study, continuous experiments for CIP degradation under optimal conditions obtained in batch experiments was investigated. Table 2 shows the CIP degradation rate in the column containing the catalyst. According to the table, with increasing contact time from 5 to 30 min, the CIP degradation rate rises from 65% to 91.9%. This can be related to the proper contact of PMS and the catalyst for the generation of reactive species and degradation of CIP. Similar results were observed by Zhang et al. [52] for the degradation of orange G.

3.10. CIP degradation pathway

To better understand the CIP degradation pathway in the PMS/G-$CoFe_2O_4$ process, the obtained sample was analyzed by UV–Vis spectrophotometric and LC-MS techniques. CIP degradation spectra in Fig. 14a show an increase in degradation efficiency at the reaction times between 5 and 30 min due to the formation of more reactive species during the PMS activation process by the catalyst. Fig. 14b shows the probable by-products of the sample extracted at the reaction time of 30 min. As can be seen, on pathway 1, by attacking $SO_4^{\bullet}$ to the CIP structure, the piperazine ring has broken and the dialdehyde product (P1 with 362 m/z) is produced. Then, this product is oxidized to the product P2 (245 m/z) by defluorination and losing the nitrogen atom. In the P2 pathway, P3 product (330 m/z) is produced by replacing the fluorine atom with the hydroxyl group. Consequently, this product is converted into a P2 product (245 m/z) by the loss of a nitrogen atom and a hydroxyl group. The products identified and their degradation pathway was similar to those reported in photocatalytic [53], PMS activated with ordered mesoporous Co_3O_4 [54] and α-MnO_2 [4].

Table 2
CIP degradation by catalyst column

Run	Initial pH	PMS dosage (mg/L)	Catalyst dosage (mM)	CIP concentration (mg/L)	Time (min)	Degradation (%)
1	7	200	2	25	5	65
2	7	200	2	25	10	72.45
3	7	200	2	25	20	80.11
4	7	200	2	25	30	91.9

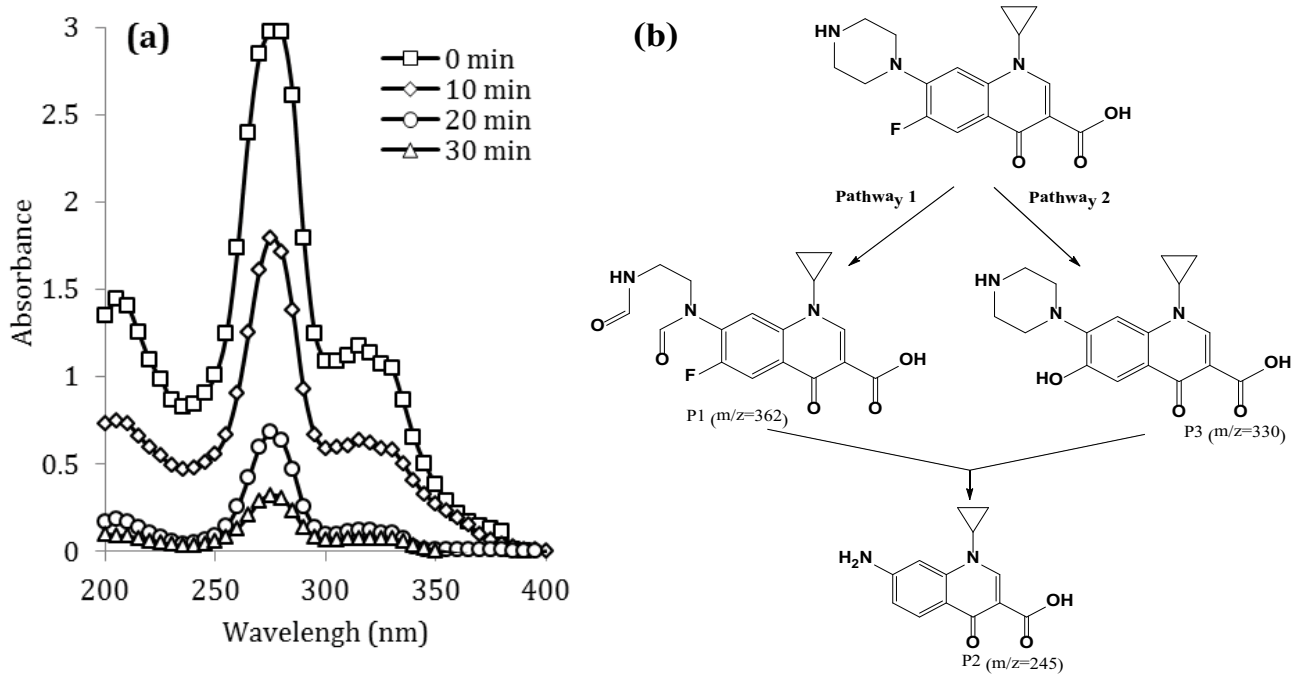

Fig. 14. Changes in the absorption spectra of CIP solution (a) and their degradation pathways (b).

4. Conclusion

The G-$CoFe_2O_4$ nanocatalyst prepared by graphene precursors, $Fe(NO_3)_3{\cdot}9H_2O$ and $Co(NO_3)_2{\cdot}6H_2O$ was characterized by SEM, EDX and XRD technologies, and was used as a PMS activator for degradation of CIP from aqueous solutions. The SEM–EDX analysis showed that graphene was effectively coated by $CoFe_2O_4$. The optimum conditions for the CIP degradation were obtained at pH of 7, G-$CoFe_2O_4$ dosage of 200 mg/L, PMS dosage of 2 mM and CIP concentration of 25 mg/L. The maximum degradation efficiency obtained in the batch and column systems under optimum conditions was 96.57% and 91.9%, respectively. The assessment of catalytic activity showed that the combination of $CoFe_2O_4$ and graphene nanoparticles resulted in the higher catalytic activity for activation of PMS and degradation of CIP compared with $CoFe_2O_4$ and Co. The constant rate of first-order kinetics for the CIP degradation process was increased by increasing the dosage of G-$CoFe_2O_4$ and PMS, but decreased by increasing the CIP concentration. The stability and reusability tests showed that G-$CoFe_2O_4$ can be used for four consecutive run cycles. The quenching experiments revealed that $SO_4^{\bullet-}$ and $^{\bullet}OH$ were produced in the PMS/G-$CoFe_2O_4$ system and $SO_4^{\bullet-}$ was the main agent for CIP degradation. As a result, the study demonstrated that the G-$CoFe_2O_4$ nanocatalyst can be considered as a promising catalyst for degradation of the CIP from aqueous solutions due to its excellent stability and reusability, and the convenient separation from the solution.

Acknowledgment

The authors are grateful for the financial support provided by the Department of Environmental Health Engineering of Isfahan University of Medical Sciences.

References

[1] B. Shen, X. Wen, G.V. Korshin, Electrochemical oxidation of ciprofloxacin in two different processes: the electron transfer process on the anode surface and the indirect oxidation process in bulk solutions, Environ. Sci. Process. Impact., 20 (2018) 943–955.

[2] A. Gupta, A. Garg, Degradation of ciprofloxacin using Fenton's oxidation: effect of operating parameters, identification of oxidized by-products and toxicity assessment, Chemosphere, 193 (2018) 1181–1188.

[3] M.S. Yahya, N. Oturan, K. El Kacemi, M. El Karbane, C. Aravindakumar, M.A. Oturan, Oxidative degradation study on antimicrobial agent ciprofloxacin by electro-Fenton process: kinetics and oxidation products, Chemosphere, 117 (2014) 447–454.

[4] J. Deng, Y. Ge, C. Tan, H. Wang, Q. Li, S. Zhou, K. Zhang, Degradation of ciprofloxacin using α-MnO_2 activated peroxymonosulfate process: effect of water constituents, degradation intermediates and toxicity evaluation, Chem. Eng. J., 330 (2017) 1390–1400.

[5] A. Wang, Y. Zhang, H. Zhong, Y. Chen, X. Tian, D. Li, J. Li, Efficient mineralization of antibiotic ciprofloxacin in acid aqueous medium by a novel photoelectro-Fenton process using a microwave discharge electrodeless lamp irradiation, J. Hazard. Mater., 342 (2018) 364–374.

[6] Y. Chen, A. Wang, Y. Zhang, R. Bao, X. Tian, J. Li, Electro-Fenton degradation of antibiotic ciprofloxacin (CIP): formation of Fe^{3+}-CIP chelate and its effect on catalytic behavior of Fe^{2+}/Fe^{3+} and CIP mineralization, Electrochim. Acta., 256 (2017) 185–195.

[7] H. Pourzamani, N. Mengelizadeh, H. Mohammadi, N. Niknam, B. Neamati, R. Rahimi, Comparison of electrochemical advanced oxidation processes for removal of ciprofloxacin from aqueous solutions, Desal. Wat. Treat., 113 (2018) 307–318.

[8] X. Zhang, R. Li, M. Jia, S. Wang, Y. Huang, C. Chen, Degradation of ciprofloxacin in aqueous bismuth oxybromide (BiOBr) suspensions under visible light irradiation: a direct hole oxidation pathway, Chem. Eng. J., 274 (2015) 290–297.

[9] M. Wang, G. Li, L. Huang, J. Xue, Q. Liu, N. Bao, J. Huang, Study of ciprofloxacin adsorption and regeneration of activated

carbon prepared from *Enteromorpha prolifera* impregnated with H_3PO_4 and sodium benzenesulfonate, Ecotoxicol. Environ. Saf., 139 (2017) 36–42.
[10] J.J.S. Alonso, N. El Kori, N. Melián-Martel, B. Del Río-Gamero, Removal of ciprofloxacin from seawater by reverse osmosis, J. Environ. Manage., 217 (2018) 337–345.
[11] A.R. Rahmani, H. Rezaei-Vahidian, H. Almasi, F. Donyagard, Modeling and optimization of ciprofloxacin degradation by hybridized potassium persulfate/zero valent-zinc/ultrasonic process, Environ. Process., 4 (2017) 563–572.
[12] A. Khan, Z. Liao, Y. Liu, A. Jawad, J. Ifthikar, Z. Chen, Synergistic degradation of phenols using peroxymonosulfate activated by CuO-Co_3O_4@MnO_2 nanocatalyst, J. Hazard. Mater., 329 (2017) 262–271.
[13] F. Gong, L. Wang, D. Li, F. Zhou, Y. Yao, W. Lu, S. Huang, W. Chen, An effective heterogeneous iron-based catalyst to activate peroxymonosulfate for organic contaminants removal, Chem. Eng. J., 267 (2015) 102–110.
[14] F. Ghanbari, N. Jaafarzadeh, Graphite-supported CuO catalyst for heterogeneous peroxymonosulfate activation to oxidize Direct Orange 26: the effect of influential parameters, Res. Chem. Intermed., 43 (2017) 4623–4637.
[15] Q. Yang, H. Choi, D.D. Dionysiou, Nanocrystalline cobalt oxide immobilized on titanium dioxide nanoparticles for the heterogeneous activation of peroxymonosulfate, Appl. Catal. B. Environ., 74 (2007) 170–178.
[16] P. Shi, R. Su, S. Zhu, M. Zhu, D. Li, S. Xu, Supported cobalt oxide on graphene oxide: highly efficient catalysts for the removal of Orange II from water, J. Hazard. Mater., 229 (2012) 331–339.
[17] Y. Yao, Z. Yang, H. Sun, S. Wang, Hydrothermal synthesis of Co_3O_4–graphene for heterogeneous activation of peroxymonosulfate for decomposition of phenol, Ind. Eng. Chem. Res., 51 (2012) 14958–14965.
[18] Y. Wang, H. Sun, H.M. Ang, M.O. Tadé, S. Wang, Magnetic Fe_3O_4/carbon sphere/cobalt composites for catalytic oxidation of phenol solutions with sulfate radicals, Chem. Eng. J., 245 (2014) 1–9.
[19] J. Liu, Z. Zhao, P. Shao, F. Cui, Activation of peroxymonosulfate with magnetic Fe_3O_4–MnO_2 core–shell nanocomposites for 4-chlorophenol degradation, Chem. Eng. J., 262 (2015) 854–861.
[20] L. Xu, W. Chu, L. Gan, Environmental application of graphene-based $CoFe_2O_4$ as an activator of peroxymonosulfate for the degradation of a plasticizer, Chem. Eng. J., 263 (2015) 435–443.
[21] Y. Li, X. Wu, Z. Li, S. Zhong, W. Wang, A. Wang, J. Chen, Fabrication of $CoFe_2O_4$–graphene nanocomposite and its application in the magnetic solid phase extraction of sulfonamides from milk samples, Talanta, 144 (2015) 1279–1286.
[22] J. Deng, Y. Shao, N. Gao, C. Tan, S. Zhou, X. Hu, $CoFe_2O_4$ magnetic nanoparticles as a highly active heterogeneous catalyst of oxone for the degradation of diclofenac in water, J. Hazard. Mater., 262 (2013) 836–844.
[23] C. Tan, N. Gao, D. Fu, J. Deng, L. Deng, Efficient degradation of paracetamol with nanoscaled magnetic $CoFe_2O_4$ and $MnFe_2O_4$ as a heterogeneous catalyst of peroxymonosulfate, Sep. Purif. Technol., 175 (2017) 47–57.
[24] Y. Xu, J. Ai, H. Zhang, The mechanism of degradation of bisphenol A using the magnetically separable $CuFe_2O_4$/peroxymonosulfate heterogeneous oxidation process, J. Hazard. Mater., 309 (2016) 87–96.
[25] Y. Wang, Y. Xie, C. Chen, X. Duan, H. Sun, S. Wang, Synthesis of magnetic carbon supported manganese catalysts for phenol oxidation by activation of peroxymonosulfate, Catalysts, 7 (2016) 3.
[26] Y. Du, W. Ma, P. Liu, B. Zou, J. Ma, Magnetic $CoFe_2O_4$ nanoparticles supported on titanate nanotubes ($CoFe_2O_4$/TNTs) as a novel heterogeneous catalyst for peroxymonosulfate activation and degradation of organic pollutants, J. Hazard. Mater., 308 (2016) 58–66.
[27] R. Tabit, O. Amadine, Y. Essamlali, K. Dânoun, A. Rhihil, M. Zahouily, Magnetic $CoFe_2O_4$ nanoparticles supported on graphene oxide ($CoFe_2O_4$/GO) with high catalytic activity for peroxymonosulfate activation and degradation of rhodamine B, RSC Adv., 8 (2018) 1351–1360.
[28] J. Deng, Y.-J. Chen, Y.-A. Lu, X.-Y. Ma, S.-F. Feng, N. Gao, J. Li, Synthesis of magnetic $CoFe_2O_4$/ordered mesoporous carbon nanocomposites and application in Fenton-like oxidation of rhodamine B, Environ. Sci. Pollut. Res., 24 (2017) 14396–14408.
[29] Y. Huang, W. Wang, Q. Feng, F. Dong, Preparation of magnetic clinoptilolite/$CoFe_2O_4$ composites for removal of Sr^{2+} from aqueous solutions: kinetic, equilibrium, and thermodynamic studies, J. Saudi. Chem. Soc., 21 (2017) 58–66.
[30] F. Zhao, Y. Zou, X. Lv, H. Liang, Q. Jia, W. Ning, Synthesis of $CoFe_2O_4$–zeolite materials and application to the adsorption of gallium and indium, J. Chem. Eng. Data., 60 (2015) 1338–1344.
[31] J. Yan, W. Gao, M. Dong, L. Han, L. Qian, C.P. Nathanail, M. Chen, Degradation of trichloroethylene by activated persulfate using a reduced graphene oxide supported magnetite nanoparticle, Chem. Eng. J., 295 (2016) 309–316.
[32] G. Rakhshandehroo, M. Salari, M. Nikoo, Optimization of degradation of ciprofloxacin antibiotic and assessment of degradation products using full factorial experimental design by Fenton homogenous process, Global NEST J., 20 (2018) 324–332.
[33] L. Gan, A. Geng, L. Xu, M. Chen, L. Wang, J. Liu, S. Han, C. Mei, Q. Zhong, The fabrication of bio-renewable and recyclable cellulose based carbon microspheres incorporated by $CoFe_2O_4$ and the photocatalytic properties, J. Cleaner Prod., 196 (2018) 594–603.
[34] J. Deng, Y.-q. Cheng, Y.-a. Lu, J.C. Crittenden, S.-q. Zhou, N.-y. Gao, J. Li, Mesoporous manganese Cobaltite nanocages as effective and reusable heterogeneous peroxymonosulfate activators for Carbamazepine degradation, Chem. Eng. J., 330 (2017) 505–517.
[35] G.-X. Huang, C.-Y. Wang, C.-W. Yang, P.-C. Guo, H.-Q. Yu, Degradation of bisphenol A by peroxymonosulfate catalytically activated with $Mn_{1.8}Fe_{1.2}O_4$ nanospheres: synergism between Mn and Fe, Environ. Sci. Technol., 51 (2017) 12611–12618.
[36] L. Lai, H. Zhou, B. Lai, Heterogeneous degradation of bisphenol A by peroxymonosulfate activated with vanadium-titanium magnetite: performance, transformation pathways and mechanism, Chem. Eng. J., 349 (2018) 633–645.
[37] J. Li, M. Xu, G. Yao, B. Lai, Enhancement of the degradation of atrazine through $CoFe_2O_4$ activated peroxymonosulfate (PMS) process: kinetic, degradation intermediates, and toxicity evaluation, Chem. Eng. J., 348 (2018) 1012–1024.
[38] L. Yang, X. Qin, X. Jiang, M. Gong, D. Yin, Y. Zhang, B. Zhao, SERS investigation of ciprofloxacin drug molecules on TiO_2 nanoparticles, Phys. Chem. Chem. Phys., 17 (2015) 17809–17815.
[39] G.P. Anipsitakis, D.D. Dionysiou, Degradation of organic contaminants in water with sulfate radicals generated by the conjunction of peroxymonosulfate with cobalt, Environ. Sci. Technol., 37 (2003) 4790–4797.
[40] C. Liu, Y. Wang, Y. Zhang, R. Li, W. Meng, Z. Song, F. Qi, B. Xu, W. Chu, D. Yuan, Enhancement of Fe@porous carbon to be an efficient mediator for peroxymonosulfate activation for oxidation of organic contaminants: incorporation NH_2-group into structure of its MOF precursor, Chem. Eng. J., 354 (2018) 835–848.
[41] S.-H. Do, J.-H. Jo, Y.-H. Jo, H.-K. Lee, S.-H. Kong, Application of a peroxymonosulfate/cobalt (PMS/Co (II)) system to treat diesel-contaminated soil, Chemosphere, 77 (2009) 1127–1131.
[42] Z. Zhao, J. Zhao, C. Yang, Efficient removal of ciprofloxacin by peroxymonosulfate/Mn_3O_4-MnO_2 catalytic oxidation system, Chem. Eng. J., 327 (2017) 481–489.
[43] Y.-H. Huang, Y.-F. Huang, C.-i. Huang, C.-Y. Chen, Efficient decolorization of azo dye Reactive Black B involving aromatic fragment degradation in buffered Co^{2+}/PMS oxidative processes with a ppb level dosage of Co^{2+}catalyst, J. Hazard. Mater., 170 (2009) 1110–1118.
[44] S. Su, W. Guo, Y. Leng, C. Yi, Z. Ma, Heterogeneous activation of Oxone by $Co_xFe_{3-x}O_4$ nanocatalysts for degradation of rhodamine B, J. Hazard. Mater., 244 (2013) 736–742.
[45] J. Li, Y. Ren, F. Ji, B. Lai, Heterogeneous catalytic oxidation for the degradation of *p*-nitrophenol in aqueous solution by persulfate activated with $CuFe_2O_4$ magnetic nano-particles, Chem. Eng. J., 324 (2017) 63–73.

[46] Y. Yao, Z. Yang, D. Zhang, W. Peng, H. Sun, S. Wang, Magnetic $CoFe_2O_4$–graphene hybrids: facile synthesis, characterization, and catalytic properties, Ind. Eng. Chem. Res., 51 (2012) 6044–6051.
[47] X. Zhou, P. Shi, Y. Qin, J. Fan, Y. Min, W. Yao, Synthesis of Co_3O_4/graphene composite catalysts through CTAB-assisted method for Orange II degradation by activation of peroxymonosulfate, J. Mater. Sci. Mater. Electron., 27 (2016) 1020–1030.
[48] L. Lai, J. Yan, J. Li, B. Lai, Co/Al_2O_3-EPM as peroxymonosulfate activator for sulfamethoxazole removal: performance, biotoxicity, degradation pathways and mechanism, Chem. Eng. J., 343 (2018) 676–688.
[49] C. Tan, N. Gao, Y. Deng, J. Deng, S. Zhou, J. Li, X. Xin, Radical induced degradation of acetaminophen with Fe_3O_4 magnetic nanoparticles as heterogeneous activator of peroxymonosulfate, J. Hazard. Mater., 276 (2014) 452–460.
[50] N.M. Julkapli, S. Bagheri, Graphene supported heterogeneous catalysts: an overview, Int. J. Hydrog. Energy., 40 (2015) 948–979.
[51] P. Shi, R. Su, F. Wan, M. Zhu, D. Li, S. Xu, Co_3O_4 nanocrystals on graphene oxide as a synergistic catalyst for degradation of Orange II in water by advanced oxidation technology based on sulfate radicals, Appl. Catal. B. Environ., 123 (2012) 265–272.
[52] J. Zhang, M. Chen, L. Zhu, Activation of peroxymonosulfate by iron-based catalysts for orange G degradation: role of hydroxylamine, RSC Adv., 6 (2016) 47562–47569.
[53] M. Chen, J. Yao, Y. Huang, H. Gong, W. Chu, Enhanced photocatalytic degradation of ciprofloxacin over Bi_2O_3/$(BiO)_2CO_3$ heterojunctions: efficiency, kinetics, pathways, mechanisms and toxicity evaluation, Chem. Eng. J., 334 (2018) 453–461.
[54] J. Deng, M. Xu, S. Feng, C. Qiu, X. Li, J. Li, Iron-doped ordered mesoporous Co_3O_4 activation of peroxymonosulfate for ciprofloxacin degradation: performance, mechanism and degradation pathway, Sci. Total Environ., 658 (2019) 343–356.